High Efficiency Converter with Charge Pump and Coupled Inductor for Wide Input Photovoltaic AC Module Applications

Wensong Yu, *Member, IEEE*, Chris Hutchens, Jih-Sheng Lai, *Fellow, IEEE*,
Jianhui Zhang, Gianpaolo Lisi, Ali Djabbari, Greg Smith, and Tim Hegarty

Abstract -- Existing photovoltaic (PV) panels have widely varying input voltages based on the panel configuration and size. In this paper, a novel topology with a single active switch – combining boost, flyback, and charge-pump circuits – is proposed in order to achieve wide input range, high voltage gain, high efficiency, and low cost simultaneously. It meets the input-voltage and power-level needs of the majority of modern PV panels while still being suitable for connection with a high-voltage dc bus. The circuit has been designed, simulated, and implemented with the 20 to 70 V input, 200±20 V output, and 220 W output power as a part of a PV ac module. Experimental results verify the validity of the novel circuit and show 97.4% peak efficiency and greater than 96.3% for 50 to 220 W.

***Index Terms* – High voltage gain, DC-DC converter, charge pump, coupled inductor, AC module, photovoltaic systems**

I. INTRODUCTION

PV ac module has been proposed as a trend for future PV systems [1-4]. Advantages of using an ac module include more flexibility in system expansion, less installation cost, lower manufacturing cost through mass production, and higher system-level energy harnessing ability under shaded conditions, since each individual PV panel can be operated at the maximum power point as compared to the single- or multi- string inverters. The ac module is intended to integrate a commercially available PV panel, typical power level less than 300 W, with a power conditioning system. A number of inverter topologies for PV ac module applications have been reported so far with respect to the number of power stages, location of power-decoupling capacitors, use of transformers, and types of grid interface [5-15]. Unfortunately, these solutions suffer from one or more of the following major drawbacks: (1) the limited-lifetime issue of electrolytic capacitors for power decoupling [5-9]; (2) limited input voltage range for the available panels in the market [10-12]; (3) high ground leakage current when the common unipolar pulse-width-modulation (PWM) scheme is used in a transformer-less PV system [13]; (4) low system efficiency if an additional high-frequency bidirectional converter is employed [14-16]; and (5) increased cost and complexity of the circuit if energy in the transformer leakage inductance is recycled by either an active snubber or soft-switching circuit [17-19].

Since galvanic insulation in an ac module for PV application is not required by code, a non-isolated ac module combining a non-isolated high step-up converter and a high-efficiency inverter with H6-type configuration, as shown in Fig. 1, can be used to solve the above issues. We reported a 98.1% European Union efficiency inverter with H6-type configuration using MOSFETs for all active switches, which features low ground leakage current, no need for split capacitors, and low output ac-current distortion, as the second power stage of a PV ac module in [20]. This paper concentrates on the first power stage – the non-isolated, high step-up, dc-dc converter.

References [21-24] presented a variety of converters using the combination of boost and flyback converters, where the boost converter section utilizes the transformer winding to achieve high voltage-conversion ratio. The leakage inductance energy of the flyback transformer is captured in the passive clamp circuit of the boost converter in order to lower the voltage-stress of the active switch. The primary current of these circuits needs to discontinuous, resulting in higher input current ripple. References [25-26] proposed a series of high boost-ratio switched-capacitor converters, where capacitor-diode voltage-multiplier circuits were adopted. These topologies have no coupled magnetics so the size and weight can be reduced. The problem is high conduction losses due to the diodes in series with the high current loop. References [27-28] proposed a combination of a high step-up converter with coupled magnetics and switched-capacitor. Thus, a higher boost ratio can be achieved while the switch current stress remains low. The problem is when the input voltage range is wide, the duty cycle needs to stretch to the upper or lower limit, which makes it difficult to optimize the design for the entire range. Moreover, the circuits have the problem to filter out the low frequency ripple in the input side if a large inductor is not used in the high voltage dc link [29].

In this paper, a novel topology with a single active switch – combining boost, flyback, and charge-pump circuits – is proposed in order to achieve wide input range, high voltage gain, high efficiency, and low cost simultaneously. Detailed circuit operation is described with topological changes in

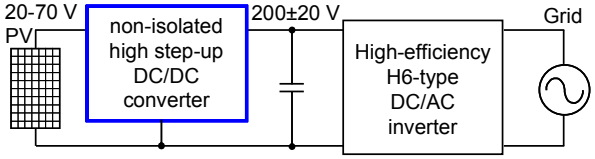

Fig. 1 PV ac module application of the proposed converter

each stage of state transitions. Voltage gain and maximum voltage stress across semiconductors in the proposed converter are derived in continuous-conduction mode. To verify the proposed approach, a 220-W hardware prototype has been designed, fabricated and tested. Experimental results verify the effectiveness of the proposed approach with 20-70 V input range, 2.9-10 times voltage gain, and 97.4% peak efficiency for photovoltaic ac module applications.

II. Basic Operational Principles of the Novel Converter

Fig.2 shows the circuit diagram of the proposed converter, which is composed of one power MOSFET, one coupled inductor, three diodes, and four capacitors. The main configuration features are that a charge pump capacitor C_{pump} is connected directly across the primary and secondary sides of the coupled-inductor and that a junction point of the clamp capacitor C_c is connected indirectly with the primary side of the coupled-inductor via the clamp diode D_c, and also to the secondary side of the coupled-inductor though the charge pump diode D_{pump}. The polarity of the coupled inductor windings is illustrated by the conventional dot symbols.

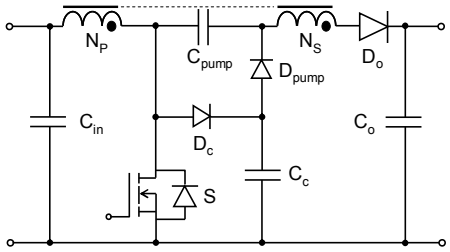

Fig. 2 Circuit diagram of the proposed converter

This proposed circuit combines the behavior of three different converter topologies: boost, flyback, and charge-pump. The flyback aspect of the topology allows the design to be optimized in terms of the transformer turns-ratio, allowing for much higher voltage gains than would be possible with a boost converter. However, flyback converters are notoriously inefficient and are very sensitive to leakage inductance, which can cause undue voltage-stress on switches and diodes. By using a clamp-circuit – identical to the output of a boost-converter – after the main switch, much of the efficiency issues can be resolved and the transformer design becomes less complicated. Finally, adding a charge-pump capacitor across the primary and secondary windings of the transformer gives higher converter voltage-gain and reduced peak current stress by allowing the current of the primary-windings to continuous.

The equivalent circuit and key waveforms of the proposed converter are illustrated in Fig. 3. The coupled inductor is modeled as a magnetizing inductor L_m, an ideal transformer with a turns ratio of N_S:N_P, primary leakage inductor L_{Lk1} and secondary leakage inductor L_{Lk2}. The voltage waveform v_{gs} is the gating signal of the active switch S; i_{Cc} is the current of the clamp capacitor C_c; i_{LK1} is the current of the primary leakage inductor; i_{Lm} is the current of the magnetizing inductor L_m; the i_{LK2} is the current of the secondary leakage inductor; the v_{ds} is the drain-to-source voltage of the active switch S; the v_{Cc} is the voltage of the clamp capacitor C_c; the v_{Do} is the voltage of the output diode D_o; the v_{Cpump} is the voltage of the charge pump capacitor C_{pump}; the v_{Lm} is the voltage waveform of the magnetizing inductor L_m.

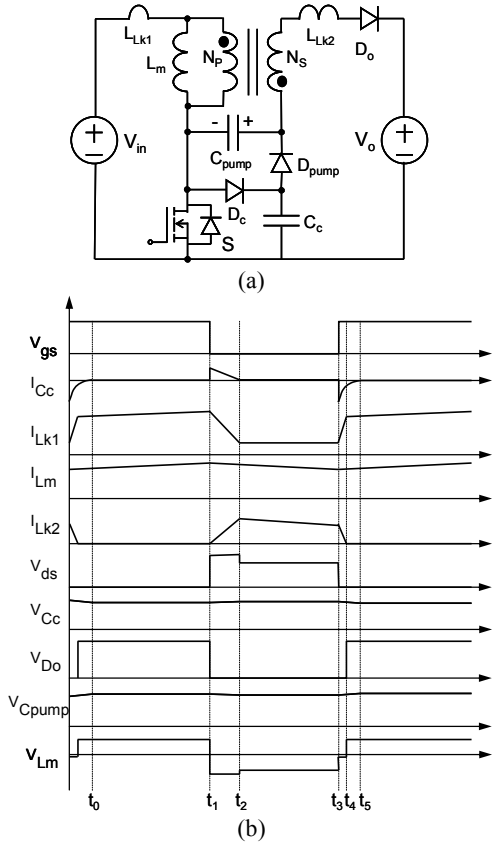

Fig. 3 Basic principle of the proposed converter: (a) equivalent circuit; and (b) key waveforms.

There are five distinct modes of operation for this circuit, as shown as Fig. 4. The topological modes are briefly described as follows.

[t_0, t_1]: MOSFET is initially turned on. At t_0, The diode D_{pump} turns off. Input voltage applies to transformer primary side and the primary current i_{Lk1} increases with a rate limited by magnetizing inductance. The energy is stored in the primary winding. The clamp, pump and output circuits are idle.

[t_1, t_2]: At t_1, the active switch turns off. Primary current i_{Lk1} decreases with a rate limited by leakage inductance and the secondary current increases simultaneously. The energy in the leakage inductance of the primary side is recycled. The voltage-stress of the switch is limited by the clamp diode and capacitor. The pump diode remains off.

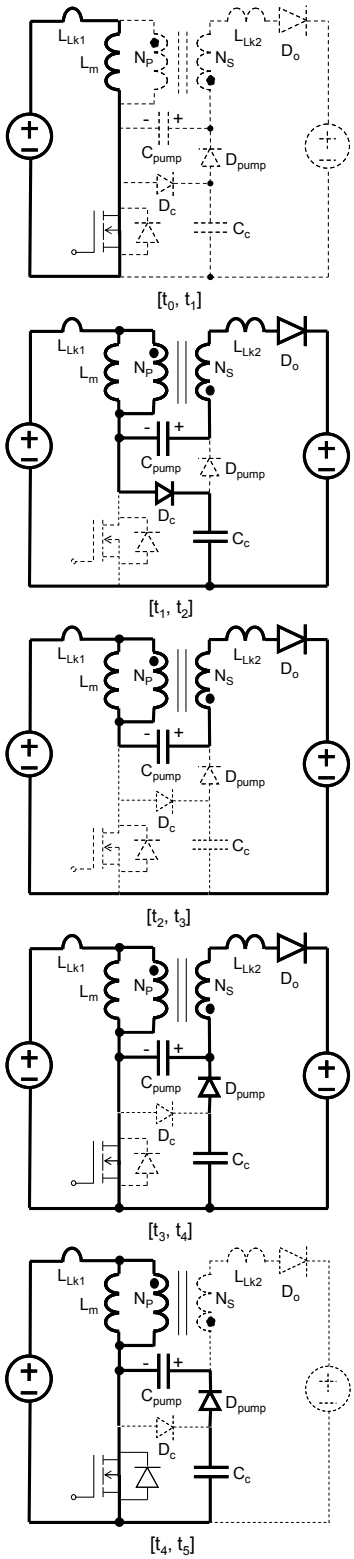

Fig. 4 Topological modes of the proposed converter

$[t_2, t_3]$: At t_2, the clamp diode turns off. The primary and secondary windings are series-connected through the pump capacitor. The primary current remains continuous and is decreasing slowly at a rate limited by the magnetizing inductance. The energy is transferred directly to the output from the input source, pump capacitor and the coupled inductor.

$[t_3, t_4]$: At t_3, active switch and the charge pump diode D_{pump} turn on. Primary current i_{Lk1} is increasing at a rate limited by the primary leakage inductance. The charge is transferred from the clamp capacitor into the pump capacitor. The secondary current is decreasing at a rate limited by the secondary leakage inductance.

$[t_4, t_5]$: At t_4, secondary current decreases to zero, output diode turns off. Charging pump diode D_{pump} remains on. Primary current i_{Lk1} increases with a rate limited by magnetizing inductance. At t_5, voltage of C_{pump} equals voltage of C_c, and the state returns to initial condition.

Fig. 5 describes the analysis results of the voltage-conversion ratio for the converter under the condition of the coupling coefficient equal to 1 when output diode D_o is on. According to the voltage-seconds balance condition of the magnetizing inductor, the voltage of the primary winding can be derived as

$$v_{pri} = V_{in} \cdot D \big/ (1-D) \tag{1}$$

And the voltage of the secondary winding is

$$v_{\sec} = \frac{N_P}{N_P} \cdot v_{pri} = V_{in} \cdot \frac{N_P}{N_P} \cdot \frac{D}{1-D} \tag{2}$$

Just like that of boost converter, the voltage of the clamp capacitor is

$$v_{Cc} = V_{in} \cdot \frac{1}{1-D} \tag{3}$$

And the voltage of the charge pump capacitor is the same as (3).

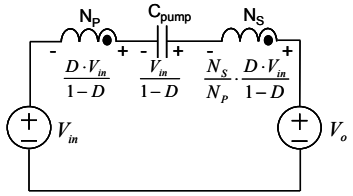

Fig. 5 Simplified voltage loop when output diode is on

According to the Fig. 5, the voltage conversion ratio can be derived as

$$\frac{V_o}{V_{in}} = \left(2 + \frac{N_S}{N_P} \cdot D\right) \Big/ (1-D) \tag{4}$$

And the voltage stress of the MOSFET, the clamp diode D_c and the pump diode D_{pump} is

$$V_{ds} = V_{Dc} = V_{Dpump} = \left(\frac{N_S}{N_P} \cdot V_{in} + V_o\right) \Big/ \left(\frac{N_S}{N_P} + 2\right) \tag{5}$$

The voltage stress of the output diode D_o can be expressed as

$$V_{Do} = \left(\frac{N_S}{N_P} \cdot V_{in} + V_o\right)\left(\frac{N_S}{N_P} + 1\right) \Big/ \left(\frac{N_S}{N_P} + 2\right) \tag{6}$$

In order to reduce the inrush current of the charge pump current loop, as shown in Fig. 4 during the $[t_3, t_4]$ interval, it is possible to insert a small inductor in the charge pump

current loop just like what switched-capacitor resonant converters do [9]. There are three optional places for the insertion of the small inductor L_{aux}, as shown in Fig. 6 (a) - (c).

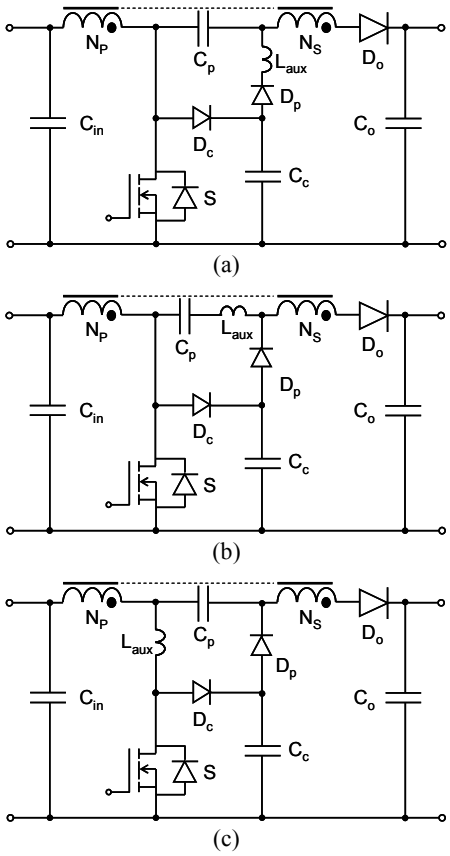

Fig. 6 Three optional places for the insertion of the inductor L_{aux}

III. Experimental Results

Fig. 7 shows the prototype photograph of the charge-pumped high step-up converter targeted at PV ac module application. As shown in Fig. 8, the implemented circuit of the prototype has the following parameters: 20-70 V input voltage, 200 V output voltage, 11-220 W output power, and 85-kHz switching frequency. The transformer core size is equivalent to ETD 39, N_P = 10 T, N_S = 27 T, L_m=24 μH, L_{Lk1}=0.4 μH, L_{Lk2}=3.1 μH. The clamping capacitor C_C and charge-pump capacitor C_{pump} are X7R 2×4.7μF. The small inductor L_{aux} is 75 nH. The output capacitor C_O is 2×22μF film capacitor. The active switch is 100-V, 9-mΩ MOSFET (FDB3632). The clamping diode D_C and charge-pump diode D_P are 100-V, 10-A Schottky diode (STPS10AH100). The output diode D_O is 600-V, 12-A ultra fast reverse recovery diode (15ETH06S). A small auxiliary diode D_{aux} (1A/600V), a snubber capacitor C_{aux}(10nF/300V), and a Zener diode D_z (0.5 W/200V) are used as a partial-loss-recovery snubber for the output diode.

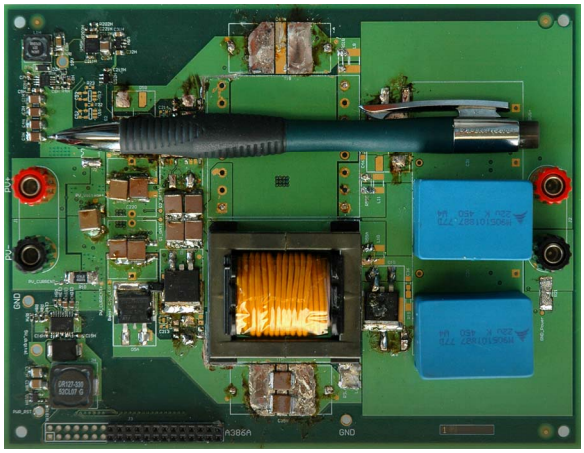

Fig. 7 Prototype photograph of the proposed high step-up converter

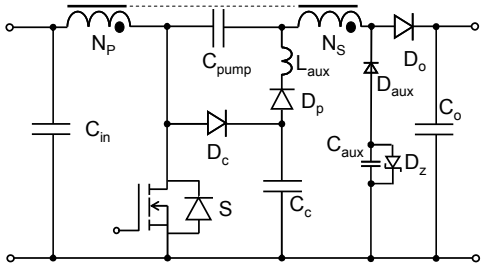

Fig. 8 Implemented circuit of the prototype

Fig. 9 shows the experimental waveforms of the pumped capacitor current and voltage under the 45 V input and 200 V output voltage, and 1 A output current conditions. It can be seen that no severe inrush current in the charge pump circuit and the voltage stress of the pump capacitor is less than 100 V. So, the compact ceramic capacitor can be used as the pump capacitor.

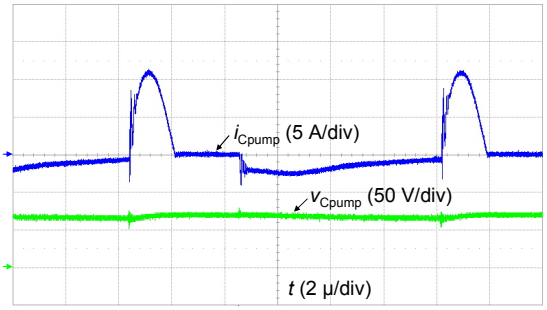

Fig. 9 Experimental waveforms of the pump capacitor current and voltage

Fig.10 (a)-(c) highlight the experimental verification for the active-device voltage and current, primary- and secondary-current at 85 kHz, 200V output voltage, and 220 W output power operation under 20 V, 45 V and 70 V input voltage conditions. The experimental waveforms show a good agreement with the analysis results. It is observed that the stress of the active switch is 60-90 V, which is much less

than the 200 V output voltages. The lower the input voltage is, the less voltage stress of the active switch. Additionally, it is found that the primary current does not drop to zero and has reduced peak current stress for the primary-windings and input filter.

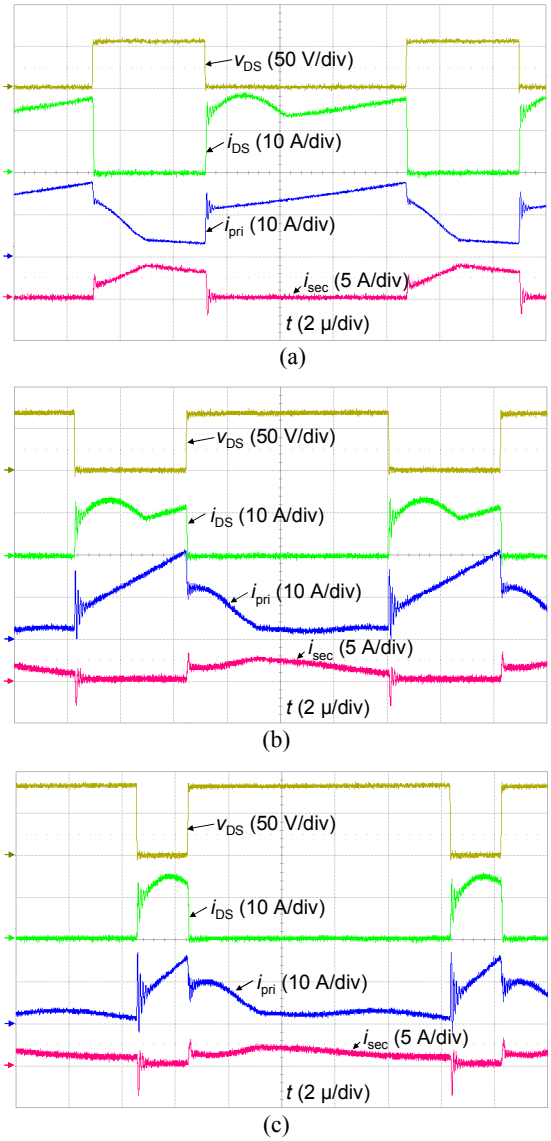

Fig. 10 Experiment verification for active device voltage and current, primary and secondary current: (a) 20V input voltage; (b) 45 V input voltage and (b) 70 V input voltage

Fig. 11 shows the experimental results of the output diode voltage stress in the worst case – maximum input and output voltage, and 220 W full load conditions. It can be seen that the partial-loss-recovery snubber circuit works well by observing that the peak voltage of the output diode is less than 450 V.

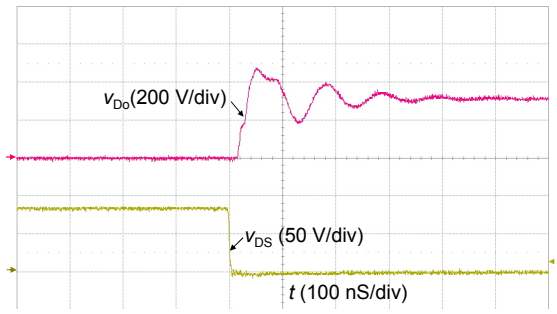

Fig. 11 Experimental results of the output diode voltage stress

Fig. 12 compares the experimental results with the calculated results of (4) showing the voltage gain as a function of the duty cycle. Both results agree with each other very well even with all the parasitics omitted in (4).

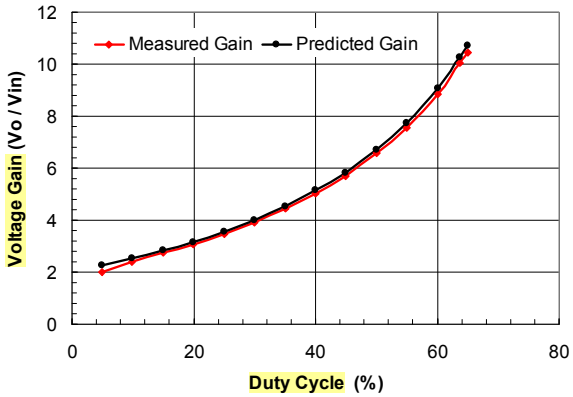

Fig. 12 Measured and predicted voltage gain.

Fig.13 describes the experimental results for efficiency under different input-voltages and output-loads with a 200-V output condition. The efficiency of the converter peaks at 97.4% and remains above 96.3% for the input voltage range of 20 to 70 V and the output power range of 50 to 220 W.

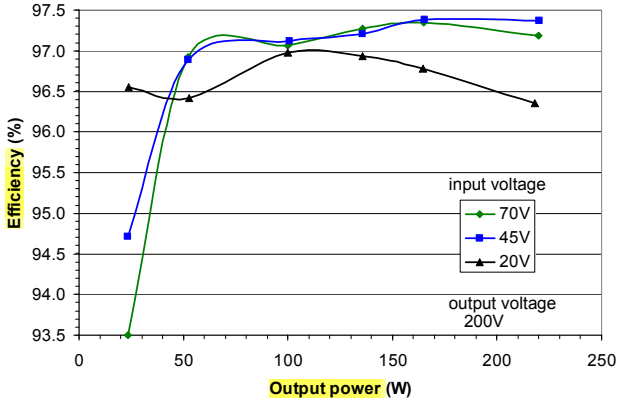

Fig. 13 Experimental results of efficiency as a function of the input voltage and the output power

IV. Conclusion

A high-efficiency dc-dc converter with a combination of

boost- and flyback-converters, including a charge-pump circuit for continuous input current operation, is proposed for wide input PV module applications. Key features of the proposed circuit are reduction of transformer and device voltage and current stresses with continuous input current, leakage inductance energy recovery, and avoiding the use of electrolytic capacitor due to reduced ripple current. The circuit has been designed, simulated, and implemented with the 20 to 70 V input, 200±20 V output, and 220 W output power as a part of a PV ac module. Experimental results verify the validity of the novel circuit and show 97.4% peak efficiency and greater than 96.3% for 50 to 220 W.

REFERENCES

[1] M. Calais, J. Myrzik, T. Spooner, and V. G. Agelidis, "Inverters for single-phase grid connected photovoltaic systems -- An overview," in *Proc. IEEE PESC'02*, vol. 2, 2002, pp. 1995-2000.

[2] F. Blaabjerg, Z. Chen, and S. B. Kjaer, "Power electronics as efficient interface in dispersed power generation systems," *IEEE Trans. Power Electron.*, vol. 19, no. 5, pp. 1184-1194, Sep. 2004.

[3] S. B. Kjaer , J. K. Pedersen and F. Blaabjerg "A review of single-phase grid-connected inverters for photovoltaic modules," *IEEE Trans. Ind. Appl.*, vol. 41, pp. 1292, Sep./Oct. 2005.

[4] Quan Li; and P. Wolfs, "A review of the single phase photovoltaic module integrated converter topologies with three different dc link configurations," *IEEE Trans. Power Electron.*, vol. 23, no. 3, pp. 1320-1333, May 2008.

[5] M. Fornage, "Method and apparatus for converting direct current to alternating current," U.S. Patent 2007 0 221 267 A1, Sep. 27, 2007.

[6] S. Saha and V. P. Sundarsingh, "Novel grid-connected photovoltaic inverter," *Proc. Inst. Elect. Eng.*, vol. 143, pp. 219-224, Mar. 1996.

[7] A. Lohner, T. Meyer, and A. Nagel, "A new panel-integratable inverter concept for grid-connected photovoltaic systems," in *Proc. IEEE ISIE'96*, vol. 2, 1996, pp. 827-831.

[8] S. B. Kjaer and F. Blaabjerg, "Design optimization of a single phase inverter for photovoltaic applications," in *Proc. IEEE PESC'03*, vol. 3, 2003, pp. 1183-1190.

[9] A. C. Kyritsis, E. C. Tatakis, and N. P. Papanikolaou, "Optimum design of the current-source flyback inverter for decentralized grid-connected photovoltaic systems," *IEEE Trans. Energy Conversion,* vol. 23, no.1 pp. 281-293, Mar. 2008.

[10] B. Sahan, A. N. Vergara, N. Henze, A. Engler and P. Zacharias, "A single-stage PV module integrated converter based on a low-power current-source inverter," *IEEE Trans. Ind. Electron.*, vol. 55,no. 7, pp. 2602-2609, Jul. 2008.

[11] H. Patel and V. Agarwal, "A single-stage single-phase transformer-less doubly grounded grid-connected PV interface," *IEEE Trans. Energy Conversion,* vol. 24, no. 1 Mar. 2009.

[12] S. Funabiki , T. Tanaka and T. Nishi "A new buck-boost-operation-based sinusoidal inverter circuit," in *Proc. IEEE PESC* ,2002, pp. 1624-1629.

[13] J. M. Chang, W. N. Chang and S. J. Chiang, "Single-phase grid-connected PV system using three-arm rectifier-inverter," *IEEE Trans. Aerosp. and Electron. Syst.,* vol. 42, no. 1, pp. 211-219, Jan. 2006.

[14] A. C. Kyritsis, N. P. Papanikolaou and E.C. Tatakis, "Enhanced current pulsation smoothing parallel active filter for single stage grid-connected AC-PV modules," in *Proc. IEEE EPE-PEMC'2008*, 1-3 Sept. 2008, pp. 1287 - 1292.

[15] T. Shimizu , K. Wada and N. Nakamura, "Flyback-type single-phase utility interactive inverter with power pulsation decoupling on the dc input for an ac photovoltaic module system," *IEEE Trans. Power Electron.*, vol. 21, pp. 1264-1272, Sep. 2006.

[16] P.T. Krein and R.S. Balog, "Cost-effective hundred-year life for single-phase inverters and rectifiers in solar and LED lighting applications based on minimum capacitance requirements and a ripple power port," in *Proc. IEEE APEC 2009,* Washington, DC, 15-19 Feb. 2009, pp. 620 - 625.

[17] Q. Li and P. Wolfs, "A current fed two-inductor boost converter with an integrated magnetic structure and passive lossless snubbers for photovoltaic module integrated converter applications," *IEEE Trans. Power Electron.*, vol. 22, no. 1, pp. 309-320, Jan. 2007.

[18] M. Andersen and B. Alvsten, "200 W low cost module integrated utility interface for modular photovoltaic energy systems," in *Proc. IEEE IECON*, 1995, pp. 572-577.

[19] C. Rodriguez and G. Amaratunga, "Long-lifetime power inverter for photovoltaic AC modules," *IEEE Trans. Ind. Electron.*, vol. 55,no. 7, pp. 2593-2601, Jul. 2008.

[20] W. Yu, J.-S. Lai, H. Qian, C. Hutchens, J. Zhang, G. Lisi, A. Djabbari, G. Smith and T. Hegarty, "High-efficiency inverter with H6-type configuration for photovoltaic non-isolated ac module applications," Submitted to *IEEE APEC 2010,* Palm Springs, CA, Feb. 21-25, 2010.

[21] E.J. Copple, "High efficiency DC step-up voltage converter," U.S. Patent 5 929 614, Jul. 27, 1999.

[22] Q. Zhao and F.C. Lee, "High-efficiency, high step-up dc-dc converters," *IEEE Trans. Power Electron.*, vol. 18, no. 1, Jan. 2003, pp. 65-72.

[23] K.C. Tseng, and T.J. Liang, "Novel high-efficiency step-up converter," *IEE Proc.-Electr. Power Appl.*, vol. 151, no. 2, Mar. 2004, pp. 182-190.

[24] D.M. Van de Sype, K.D. Gussemé, B. Renders, A.P. Van den Bossche, and J.A. Melkebeek, "A Single switch boost converter with a high conversion ratio," *in Proc. of IEEE APEC,* Mar.2005, pp. 1581-1587.

[25] Y.P.B. Yeung, K.W.E. Cheng, S.L. Ho, K.K. Law, and D. Sutanto, "Unified analysis of switched-capacitor resonant converters," *IEEE Trans. Ind. Electron.*, vol. 51, no. 4, Aug. 2004, pp. 864-873,.

[26] E.H. Ismail, M.A. Al-Saffar, A.J. Sabzali, and A.A. Fardoun, "A family of single-switch PWM converters with high step-up conversion ratio," *IEEE Trans. Circuits Syst.*, vol. 55, no. 4, May 2008, pp. 1159-1171.

[27] R.J. Wai and R.Y. Duan, "Boost converter utilizing bi-directional magnetic energy transfer of coupling inductor," U.S. Patent 7 161 331, Apr. 11, 2005.

[28] J.W. Baek, M.H. Ryoo, T.J. Kim, D.W. Yoo, and J.S. Kim, "High boost converter using voltage multiplier," *in Proc. of IEEE IECON,* Nov.2005, pp. 567-572

[29] R. J. Wai , C. Y. Lin , R. Y. Duan and Y. R. Chang "High-efficiency power conversion system for kilowatt-level stand-alone generation unit with low input voltage," *IEEE Trans. Ind. Electron.*, vol. 55, no. 10 pp. 3702-3714, Oct. 2008.